Spatial variation in mechanical properties along the sciatic and tibial nerves: an ultrasound shear wave elastography study

Ricardo J. Andrade, Sandro Freitas, François Hug, Michel Coppieters, Eva Sierra-Silvestre, Antoine Nordez

Spatial variation in mechanical properties along the sciatic and tibial nerves: An ultrasound shear wave elastography study

Ricardo J. Andrade [a,b,c], Sandro R. Freitas [d], François Hug [a,e,f,g], Michel W. Coppieters [b,h], Eva Sierra-Silvestre [c], Antoine Nordez [a,f,i,*]

[a] Nantes Université, Movement - Interactions - Performance, MIP, UR 4334, F-44000 Nantes, France
[b] Menzies Health Institute Queensland, Griffith University, Brisbane and Gold Coast, Australia
[c] School of Health Sciences and Social Work, Griffith University, Brisbane and Gold Coast, Australia
[d] Neuromuscular Research Lab, Faculdade de Motricidade Humana, Universidade de Lisboa, Portugal
[e] Université Côte d'Azur, LAMHESS, Nice, France
[f] Institut Universitaire de France (IUF), Paris, France
[g] School of Health and Rehabilitation Sciences, The University of Queensland, Brisbane, Australia
[h] Department of Human Movement Sciences, Faculty of Behavioural and Movement Sciences, Vrije Universiteit Amsterdam, Amsterdam Movement Sciences, Amsterdam, the Netherlands
[i] Health and Rehabilitation Research Institute, Faculty of Health and Environmental Sciences, Auckland University of Technology, Auckland, New Zealand

ARTICLE INFO

Keywords:
Ultrasound shear wave elastography
Ultrasonography
Sciatic neuropathy
Peripheral nervous system
Nerve biomechanics
Non-invasive mechanics
Mononeuropathies
Diagnostic imaging

ABSTRACT

Ultrasound shear wave elastography has become a promising method in peripheral neuropathy evaluation. Shear wave velocity, a surrogate measure of stiffness, tends to increase in peripheral neuropathies regardless of etiology. However, little is known about the spatial variation in shear wave velocity of healthy peripheral nerves and how tensile loading is distributed along their course. Sixty healthy young adults were scanned using ultrasound shear wave elastography. Five regions of the sciatic (Sciatic $_{PROXIMAL}$, Sciatic $_{DISTAL}$) and tibial nerve (Tibial $_{PROXIMAL}$, Tibial $_{INTERMEDIATE}$, and Tibial $_{DISTAL}$) were assessed in two hip positions that alter nerve tension: 1) neutral in supine position; and 2) flexed at 90°. Knee and ankle remained in full-extension and neutral position. We observed spatial variations in shear wave velocity along the sciatic and tibial nerve ($P < 0.0001$). Shear wave velocities were significantly different between all nerve locations with the exception of Sciatic $_{DISTAL}$ vs. Tibial $_{INTERMEDIATE}$ ($P = 0.999$) and Tibial $_{PROXIMAL}$ vs. Tibial $_{INTERMEDIATE}$ ($P = 0.708$), and tended to increase in the proximal-distal direction at both upper and lower leg segments. Shear wave velocity increased with hip flexion (+54.3%; $P < 0.0001$), but the increase was not different among nerve locations ($P = 0.233$). This suggests that the increase in tensile loading with hip flexion is uniformally distributed along the nerve tract. These results highlight the importance of considering both limb position and transducer location for biomechanical and clinical assessments of peripheral nerve stiffness. These findings provide evidence about how tension is distributed along the course of sciatic and tibial nerves.

1. Introduction

Various animal models of peripheral neuropathies, such as those associated with metabolic syndrome (Layton et al., 2004), trauma (Zhu et al., 2020) or anti-neoplastic drugs (Bober and Shah, 2015), have shown that peripheral nerve stiffness tends to be higher regardless of etiology. Using ultrasound shear wave elastography, preliminary human studies have demonstrated that shear wave velocity of nerves, a surrogate measure of nerve stiffness (Schrier et al., 2020), increases in both compression (Kantarci et al., 2014) and diabetic (Dikici et al., 2016) neuropathies. However, these clinical investigations focused on a single nerve region and did not account for potential heterogeneity of mechanical changes along the course of peripheral nerves. Although spatial heterogeneity in shear wave velocity has recently been reported in healthy upper limb nerves (Greening and Dilley, 2017; Rugel et al., 2020), a comprehensive elasticity mapping of sciatic and tibial nerves

* Corresponding author at: Nantes Université, Movement - Interactions - Performance, MIP, UR 4334, 25 Bis Boulevard Guy Mollet, BP 72206, 44322 Nantes, France.
E-mail address: antoine.nordez@univ-nantes.fr (A. Nordez).

remains to be investigated.

Length-dependent neuropathies, such as diabetic polyneuropathy, are typically characterized by clinical manifestations primarily located distally, but with a proximal progression (Watson and Dyck, 2015). Furthermore, similar to remote neuro-immune inflammatory findings observed in focal mononeuropathies (Schmid et al., 2013), increased sciatic nerve shear wave velocity has also been reported far away from the lesion site in lumbar radiculopathies (Çelebi et al., 2019; Neto et al., 2019; Wang et al., 2019). Collectively, these observations highlight a need for improved understanding of the spatial variations in ultrasound shear wave velocity along the course of peripheral nerves which could improve the ability to distinguish normal regional differences in nerve mechanical properties from those arising from damage and, potentially, regeneration.

It has previously been suggested that healthy peripheral nerves exhibit regional variations in their ultrastructure, including number of fascicles (Sunderland, 1945; Sunderland and Ray, 1948), proportion of epineural tissue (Sunderland, 1990) and collagen fibre diameter (Mason and Phillips, 2011), which likely to ditacte the shear wave velocity. Peripheral nerves undergo considerable mechanical loads during limb movements and body postures (Boyd and Dilley, 2014; Ellis et al., 2017). Both animal (Phillips et al., 2004) and cadaver (Mahan et al., 2015) studies reported that healthy peripheral nerves exhibit heterogeneous mechanical responses to (physiological) tensile stresses, being this response influenced by a nerve's proximity to joint regions. Shear wave velocity, as measured by using ultrasound shear wave elastography, is also a good indicator of tensile loading of soft tissues (Hug et al., 2015) such as peripheral nerves (Andrade et al., 2016). For example, recent studies have demonstrated that nerve-directed movements or limb positions can modulate the shear wave velocity of healthy human nerves (Andrade et al., 2020; Andrade et al., 2016; Rugel et al., 2020). However, it remains unclear how shear velocity varies along the length of resting healthy nerves in-vivo, and how it behaves under tensile loads (i.e., stretching).

Despite utrasound shear wave elastography has become a promising non-invasive method for characterising changes in peripheral nerve mechanics that are associated with altered tissue structure and composition (Wee and Simon, 2019), the spatial variations in mechanical properties of healthy nerves are not well understood in-vivo. This study aimed to: 1) investigate the spatial variations in shear wave velocity along the sciatic and tibial nerve in healthy individuals; and 2) examine the influence of tensile loading on the spatial variations in shear wave velocity. Based on structural (Mason and Phillips, 2011) and mechanical (Mahan et al., 2015; Phillips et al., 2004) findings from both animal and cadaver studies, we hypothesized that sciatic and tibial nerve would exhibit regional differences in shear wave velocity along their length and that tensile loading would not be uniformly distributed.

2. Methods

We analyzed data collected at baseline of a published randomized controlled study (Andrade et al., 2020). Considering the large number of outcome measures and main study purposes, the analysis of the spatial variations in shear wave velocity were not examined in the previous publication.

2.1. Participants

Sixty healthy young adults (29 females, 31 males; age: 20.5 ± 2.0 years, height: 172.2 ± 9.1 cm, weight: 63.8 ± 9.0 kg) with no self-reported history of lower limb neuropathy, or musculoskeletal disorders, participated in this study. Prior to testing, written informed consent was obtained from all participants. The study was approved by the Institutional Ethics Review Board.

2.2. Shear wave elastography acquisition

Ultrasound shear wave elastography provides real-time and high spatial resolution elasticity mapping by measuring the propagation velocity of shear waves generated remotely using ultrasonic focused beams (Gennisson et al., 2013). Nerve shear wave velocities are typically used as a surrogate measure of musculoskeletal tissue stiffness (Hug et al., 2015). Considering an elastic, homogeneous and isotropic medium, the relationship between the shear wave velocity (V^2) and the shear modulus (μ) arise from the following equation: $\mu = \rho V^2$, where ρ is the density (assuming $\rho = 1000$ kg m^{-3}) (Bercoff et al., 2004). The Young's modulus (E) can then be derived from the following equation: $E = 3\mu$. Preliminary shear wave elastography studies on peripheral nerves have reported outcomes in either shear modulus (Dikici et al., 2016; Paluch et al., 2018) or shear wave velocity (Andrade et al., 2020; Neto et al., 2019) as commercial systems can display all these metrics. However, the Young's modulus calculation from the shear wave velocity do not hold for anisotropic musculoskeletal tissues, such as the peripheral nerves (Gennisson et al., 2010). In addition, for a thin and stiff layer, the propagation of the shear waves can be guided (i.e., when they experience successive reflections on the nerve boundaries) and this phenomena has the potential to affect the relationship between the shear modulus and the shear wave velocity (Brum et al., 2014). For this reason, this study reports the values in terms of shear wave velocity, and we further examined the influence of nerve thickness on nerve shear wave velocity.

A 38-mm linear array transducer (*L*10-2 MHz; Super Linear, Aix-en-Provence, France) coupled to an Aixplorer ultrasound scanner (version 6.1; Supersonic Imagine, Aix-en-Provence, France) was used for all measurements. Shear wave elastography scans were performed in MSK preset with penetration mode, 100% opacity, no temporal smoothing (persistence = OFF), and intermediate spatial smoothing − 5/9. All ultrasound data were collected by the same experienced examiner (RJA) using minimal transducer pressure. The maps of the shear wave velocity were obtained at 1 sample/s with a spatial resolution of 1 × 1 mm.

All ultrasound scans were performed in a single experimental session on the participant's right lower limb. Each participant was imaged in two different positions in a random order: (1) hip neutral and (2) hip flexed at 90°. For the assessments in hip neutral, participants lay prone on a dynamometer system with both hips positioned in neutral rotation (Biodex 3 Medical, NY, USA). For the assessments in hip flexion, participants sat in long sitting on the dynamometer chair. For both hip testing conditions, participant's right foot was attached to a footplate with the knee fully extended. The lateral malleolus was aligned with the axis of the dynamometer system and considered as an estimate of the center of rotation of the ankle. The ankle joint was then positioned in neutral position, defined as the angle of 90° between the footplate and the shank. For both testing positions, the contralateral limb was supported in approximately 45° knee flexion. Based on previous cadaver and shear wave elastography investigations (Coppieters et al., 2006; Greening and Dilley, 2017), the hip neutral position was expected to induce minimal axial tension on the sciatic and tibial nerve whereas hip flexion would increase substantially the nerve tension.

Spatial variations in shear wave velocity were examined along the course of the sciatic and tibial nerve. Measurements were performed at both thigh and lower leg segments. Skin markings were used to divide the sciatic and tibial nerve into five different regions for ultrasound examination purposes (Fig. 1): Sciatic $_{\text{PROXIMAL}}$, Sciatic $_{\text{DISTAL}}$, Tibial $_{\text{PROXIMAL}}$, Tibial $_{\text{INTERMEDIATE}}$, and Tibial $_{\text{DISTAL}}$. Four anatomical landmarks were used to locate these regions: (i) the midpoint between the ischial tuberosity and the greater trochanter; (ii) the point where the sciatic nerve bifurcates into tibial and common fibular nerve; (iii) the lateral femoral condyle; and (iv) the medial malleolus (Fig. 1). B-mode ultrasound was used to locate the anatomical references. The sciatic nerve was then divided into two equidistant regions between points (i) and (ii): Sciatic $_{\text{PROXIMAL}}$ and Sciatic $_{\text{DISTAL}}$. The midpoint of each region

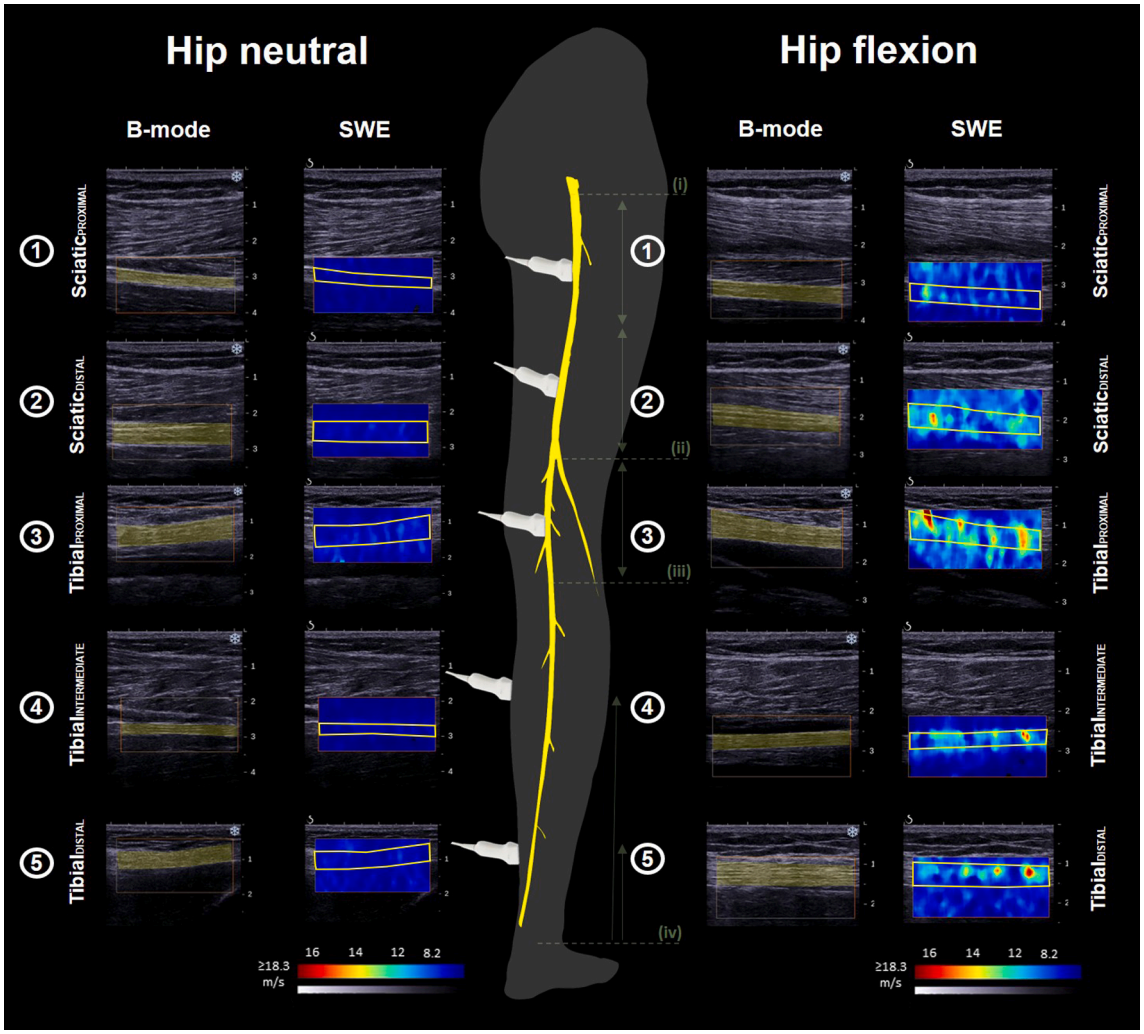

Fig. 1. Typical example of shear wave elastography measurements per nerve location and hip posture. Shear wave elastography mode allows to simultaneously acquire B-mode and shear wave elastography windows. Numbers represent the location where ultrasound scans were performed. 1: Sciatic $_{PROXIMAL}$; 2: Sciatic $_{DISTAL}$; 3: Tibial $_{PROXIMAL}$; 4: Tibial $_{INTERMEDIATE}$; 5: Tibial $_{DISTAL}$; (i) midpoint between the ischial tuberosity and the greater trochanter; (ii) the point where sciatic nerve bifurcates into tibial and common peroneal nerves; (iii) the lateral femoral condyle; and the (iv) medial malleolus.

was identified and used as a reference for transducer position. The Tibial $_{PROXIMAL}$ was imaged at the midpoint between (ii) and (iii). The distance from point (iv) and (iii) was measured. Tibial $_{INTERMEDIATE}$ and Tibial $_{DISTAL}$ were scanned at 50% and 10% of this distance, respectively.

Prior to the ultrasound assessments, five passive ankle rotations (from 40° plantar flexion to 0°) were performed at 5°/s to pre-condition the neuromusculoskeletal structures acting on ankle joint, including the sciatic and tibial nerve. This conditioning procedure was completed for both testing positions. The ankle was then passively positioned in a resting angle (neutral position) and the examination of shear wave velocity was performed in a randomized order for all the five nerve regions. Briefly, the nerve was first identified in the transverse plane. The transducer was subsequently rotated 90° into the longitudinal plane and aligned with the direction of the nerve fibers. The center of the transducer was aligned with the midpoint of each nerve region. The shear wave velocity map was placed over the nerve and its location remained unchanged during the duration of each clip. The size of the elastography map was defined as the largest size allowed by the scanner. A 10 s shear wave elastography clip was obtained for each region. After recording one clip, the transducer was then immediately moved to the next nerve region, and the procedure for data acquisition was repeated. Real-time shear wave elastography and B-mode windows (Fig. 1) were acquired simultaneously to assess both the nerve shear wave velocity (elastography window) and nerve geometry (B-mode window). The B-mode window was used to: 1) identify region of interest (ROI) for shear wave velocity calculations; and 2) measure the nerve thickness. Participants were instructed to remain completely relaxed during the ultrasound scans, and hence with their lower limb muscles in the passive state.

2.3. Data analysis

All data were analyzed offline using customized Matlab (Version 18; The MathWorks Inc, Natick, MA, USA) scripts. Data remained coded so that the data analyses could be undertaken in a blinded manner for testing position and nerve region. Shear wave elastography clips were exported in “mp4” format exported from the system. Clips were then converted (1 Hz) into JPEG images. ROIs were then manually traced (image-by-image) on the adjacent B-mode window using a custom script (ElastoGUI, Laboratory MIP, University of Nantes, France). ROIs were defined as the largest nerve area within the nerve hyperechoic boundaries (epineurium) of the sciatic and tibal nerves, a 2D approximation of the nerve structure based on its thickness. Next, each pixel of the color map (shear wave velocity) was converted into a shear wave velocity value based on the scanner’s scale (0–18.3 m/s). Shear wave velocity values within the ROI were averaged to obtain a representative shear

wave velocity value (m/s) per frame. Mean shear wave velocity extracted from each frame was then averaged over consecutive frames (total of 10 s), and this value was used for statistical analysis. The area of the ROIs was also calculated and averaged over consecutive images. The percentage of signal void (pixels within shear wave elastography map without shear wave velocity value) and saturation (pixels with maximum shear wave velocity value – 18.3 m/s) were quantified for each nerve ROI. If present, void areas were excluded from the analysis. Nerve thickness was calculated from the ROI coordinates and calibrated using a known distance on the image. Thickness was measured as the mean of six different straight lines between superficial and deep nerve boundaries (epineurium) along the longitudinal view of each nerve B-image.

2.4. Statistical analysis

All statistical analyses were conducted in GraphPad Prism (version 8; GraphPad Software, Inc., CA, US). Data are presented as mean ± standard deviation. Differences in nerve shear wave velocity and thickness were assessed using two-way repeated-measures ANOVA with nerve region (Sciatic $_{PROXIMAL}$, Sciatic $_{DISTAL}$, Tibial $_{PROXIMAL}$, Tibial $_{INTERMEDIATE}$, and Tibial $_{DISTAL}$) and hip position (hip neutral, hip flexed) as fixed factors. Post-hoc analyses were performed using Bonferroni tests for multiple comparisons. To investigate the potential influence of nerve thickness on shear wave velocity, univariate linear regression analysis was used to find the best fit line of shear wave velocity to nerve thickness. Pearson correlation coefficients were used to evaluate the relationships between nerve shear wave velocity and body heigh, weight and BMI. This analysis was performed for both Hip neutral and Hip flexed positions and included all nerve locations. The level of significance was set at $P < 0.05$.

3. Results

3.1. Shear wave velocity

We observed a low occurrence of saturated values (maximum saturation in hip neutral = 0%; maximum saturation in hip flexed = 23.1% and interquartile range = 0.4%) and very small void areas (maximum saturation in hip neutral = 0.8% and interquartile range = 0%; maximum saturation in hip neutral = 2.1% and interquartile range = 0%) on the shear wave velocity measurements (Table 1). The segmented shear wave elastography ROI area per nerve region was 1.2 ± 0.2 cm^2 for Sciatic $_{PROXIMAL}$, 1.4 ± 0.3 cm^2 for Sciatic $_{DISTAL}$,1.4 ± 0.3 cm^2 for Tibial $_{PROXIMAL}$, 1 ± 0.3 cm^2 for Tibial $_{INTERMEDIATE}$, and 0.9 ± 0.2 cm^2 for Tibial $_{DISTAL}$. There were no significant correlations between shear wave velocity and BMI or body weight. A significant weak positive correlation was found between shear wave velocity and height (data comprised all nerve regions and hip positions: r = 0.091, p = 0.027). When subgrouping by nerve region and hip position, this correlation was only positive for Sciatic $_{DISTAL}$ (grouped hip neutral and hip flexed: r = 0.23, P = 0.013; hip flexion only: r = 0.3, P = 0.018; hip neutral only: r = 0.33; P = 0.009).

There was no significant interaction between hip position and nerve region ($F(4,236) = 1.4$; $P = 0.233$) on shear wave velocity. Significant main effects of nerve region ($F(4,236) = 47.8$; $P < 0.0001$) and hip position ($F(1,59) = 310$; $P < 0.0001$) were observed. Specifically, shear wave velocity varied systematically with spatial location regardless of the hip position. Post hoc analysis revelad that shear wave velocities were significantly different between all nerve locations, with the exception of Sciatic $_{DISTAL}$ vs. Tibial $_{INTERMEDIATE}$ ($P = 0.999$) and Tibial $_{PROXIMAL}$, vs. Tibial $_{INTERMEDIATE}$ ($P = 0.708$). Overall, shear wave velocities tended to increase in the proximal–distal direction at both thigh and lower leg segments and were highest in nerve regions near the knee (Tibal $_{PROXIMAL}$) and ankle (Tibial $_{DISTAL}$) joints (Fig. 2A).

In addition, the main effect of hip position showed a large increase in shear wave velocity (+54.3 ± 45.7%, on average) when the hip was flexed compared to the neutral position (Fig. 3). The absence of significant interaction suggest that the spatial variations in shear wave velocity along the anatomic course of the nerve were not altered by the addition of tensile stress to the nerve (i.e., hip flexion). Notably, hip flexion induced a similar mean (SD) increase in shear wave velocity across all nerve regions: +2.4 ± 1.6 m/s for Sciatic $_{PROXIMAL}$; +2.8 ± 1.9 m/s for Sciatic $_{DISTAL}$; +2.9 ± 2.1 m/s for Tibial $_{PROXIMAL}$; +2.5 ± 1.9 m/s for Tibial $_{INTERMEDIATE}$, and + 2.9 ± 1.8 m/s Tibial $_{DISTAL}$.

Table 1
Shear wave velocity (m/s), percentage of ROI saturation, and percentage of ROI void areas used for shear wave elastography assessments. Data is displayed as mean ± SD for each nerve region and hip posture.

	Nerve region	Hip position	
		Hip neutral	Hip flexed
Shear wave velocity (m/s)	**Sciatic$_{PROXIMAL}$**	4.6 ± 1.2	7.1 ± 1.2
	Sciatic$_{DISTAL}$	5.7 ± 1.2	8.5 ± 1.6
	Tibial$_{PROXIMAL}$	6.5 ± 1.5	9.4 ± 2.0
	Tibial$_{INTERMEDIATE}$	5.8 ± 1.1	8.2 ± 1.7
	Tibial$_{DISTAL}$	6.2 ± 1.0	9.1 ± 1.5
ROI Saturation (%) (Number of images with ROI Saturation/Total of images analyzed)	**Sciatic$_{PROXIMAL}$**	0.0 ± 0.0 (0/60)	0.2 ± 0.4 (19/60)
	Sciatic$_{DISTAL}$	0.0 ± 0.0 (0/60)	1.2 ± 1.9 (33/60)
	Tibial$_{PROXIMAL}$	0.0 ± 0.0 (0/60)	1.3 ± 3.4 (33/60)
	Tibial$_{INTERMEDIATE}$	0.0 ± 0.0 (0/60)	0.6 ± 1.2 (22/60)
	Tibial$_{DISTAL}$	0.0 ± 0.0 (0/60)	0.4 ± 1.4 (15/60)
ROI Void (%) (Number of images with ROI Void/Total of images analyzed)	**Sciatic$_{PROXIMAL}$**	0.0 ± 0.0 (0/60)	0.1 ± 0.3 (16/60)
	Sciatic$_{DISTAL}$	0.0 ± 0.0 (0/60)	0.1 ± 0.1 (26/60)
	Tibial$_{PROXIMAL}$	0.0 ± 0.0 (0/60)	0.0 ± 0.1 (15/60)
	Tibial$_{INTERMEDIATE}$	0.0 ± 0.1 (2/60)	0.1 ± 0.3 (14/60)
	Tibial$_{DISTAL}$	0.0 ± 0.0 (0/60)	0.0 ± 0.0 (2/60)

ROI: region of interest.

3.2. Nerve thickness

The analysis of variance revealed no main effect of hip position ($F(1,59) = 1.9$; $P = 0.171$) neither an interaction between region and hip position ($F(4,236) = 1.1$; $P = 0.369$). A significant main effect of region on nerve thickness ($F(4, 236) = 87.3$; $P < 0.0001$) was observed. Overall, it suggests that nerve was thicker along the thigh than at lower leg (Fig. 3B), and that these regional differences were not significantly affected by nerve tensioning. Shear wave velocity was not significantly correlated to the nerve thickness (Hip neutral: r = 0.028, p = 0.623; Hip

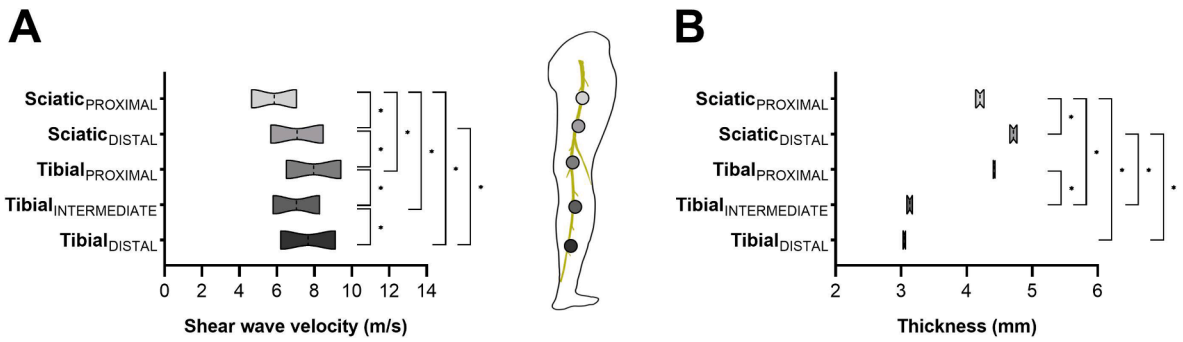

Fig. 2. Panel A. Spatial variations in shear wave velocities (m/s) across the different regions of the sciatic nerve tract: Sciatic $_{PROXIMAL}$, Sciatic $_{DISTAL}$, Tibial $_{PROXIMAL}$, Tibial $_{INTERMEDIATE}$, and Tibial $_{DISTAL}$. *P < 0.0001. **Panel B.** Spatial variations in thickness (mm) across the sciatic nerve tract. *P < 0.0001. For both panels, data corresponds to the ANOVA's effect of region and combines both hip neutral and hip flexed positions. Violin plots show.

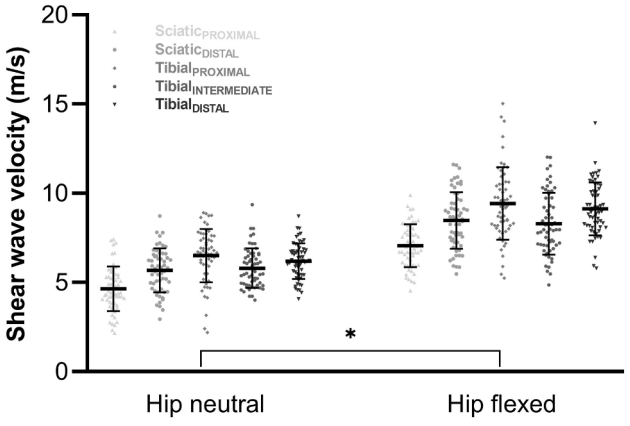

Fig. 3. Effects of hip angle position on shear wave velocity across five different regions of the sciatic nerve tract: Sciatic $_{PROXIMAL}$, Sciatic $_{DISTAL}$, Tibial $_{PROXIMAL}$, Tibial $_{INTERMEDIATE}$, and Tibial $_{DISTAL}$. Shear wave velocity was significantly greater in hip flexion compared to hip neutral position for all nerve regions. Horizontal lines correspond to the mean ± SD and individual data is shown. *P < 0.0001.

flexed: r = -0.074, p = 0.199).

4. Discussion

The results of this study show that shear wave velocity varies spatially along the course of the sciatic and tibial nerve. Shear wave velocities increased in a proximal to distal pattern at both upper and lower leg semgents. In contrast, the regional variations were not affected by the overall tensioning of the nerve. This suggests that axial tension is uniformly distributed along the course of healthy sciatic and tibial nerve when subjected to tensile loads (i.e., stretching).

Averaged shear wave velocities ranged between 4.6 and 6.5 m/s for hip neutral and 7.1–9.4 m/s and hip flexed (Table 1). These values are comparable to those described in previous studies (Andrade et al., 2016; Greening and Dilley, 2017; Neto et al., 2019) for healthy sciatic and tibial nerve. As expected, shear wave velocity increased with the hip flexion across all nerve locations which suggests an increase in sciatic and tibial nerve tensioning (Boyd et al., 2013; Coppieters et al., 2006) and demonstrates the elastic nature of peripheral nerves (Topp and Boyd, 2006). Furthermore, it highlights the importance of considering the hip position on either clinical or biomechanical assessments of lower limb nerves regardless the location where the ultrasound scans are performed.

Because of their stiff nature and finite thickness with respect to the shear wavelength, the propagation of the shear waves has been proven to be guided in tendons (Brum et al., 2014). This phenomenon cannot be excluded when assessing relatively thin peripheral nerves, and it could bias the nerve shear wave velocities. For example, a thicker nerve may be associated to a higher shear wave velocity for a given shear modulus and vice versa. We speculate that the phenomenon of guided waves may be minor in peripheral nerves for two reasons: 1) the fact that shear waves propagate much faster in tendons than in peripheral nerves; and 2) the smaller difference in shear wave velocity between nerves and the surrounding tissues, as depicted shear wave elastography maps in Fig. 1. This can be partly confirmed by the absence of correlations between the shear wave velocity and nerve thickness. In addition, our data showed that thickness was not affected by the hip angle and the nerve region with the second highest shear wave velocity (i.e., tibial $_{DISTAL}$) was also the thinnest, as opposed to the guided wave propagation behavior. We are therefore confident that the spatial variations in shear wave velocity were not biased by the guided wave behavior. However, the regional variations in nerve thickness adds a layer of complexity when interpreting the shear wave velocity mapping. As shown in Table 2, four of ten comparisons between nerve locations may have been influenced by concomitant variations in nerve thickness and nerve shear wave velocity. Future studies should investigate the influence of the guided wave behavior when using ultrasound shear wave elastography to assess the mechanical properties of peripheral nerves. Notably, six of the comparisons between locations showed significant differences in shear wave velocity that were unlikely to have been affected by nerve thickness. Based on these observations, we believe that the sciatic and tibial nerve displays large regional changes in mechanical properties.

Our results showed that shear wave velocity increased in a proximal to distal pattern at both upper and lower leg segments, being greatest in locations near knee and ankle joints (Fig. 2). This finding suggests that sciatic nerve tract exhibits heterogeneous mechanical properties along its course. These results could be due to regional variations in their ultrastructure such as thinner and more numerous nerve fascicles wrapped by a thicker perineurium near joints (Hadzic, 2017; Sunderland, 1965), and an increased epineurial tissue content at joints regions (Sunderland, 1965). Proximity to joint regions has also been associated to distinct nerve material properties (Phillips et al., 2004). For example, Tibial $_{PROXIMAL}$ was assessed on a highly mobile (knee) joint region, subjected to higher localized strains that can lead to distinct shear wave velocities. Similarly, we found spatial variations in sciatic and tibial nerve thickness (Fig. 2B). This finding strongly suggests that sciatic and tibial nerves exhibit a heterogeneous geometry as they course distally. Our nerve thickness outcomes, which are equivalent to dorsal to ventral measurement in a cross-sectional view, are in line with cadaveric (Gustafson et al., 2012) and ultrasound (Bruhn et al., 2008) findings. In particular, demonstrating that sciatic nerve is elliptical proximally and becomes circular as it courses distally.

Several studies have investigated the shear wave velocity of the sciatic nerve including the response to passive joint motion and various limb postures (Andrade et al., 2016; Greening and Dilley, 2017),

Table 2
Inter-regional comparisons for shear wave velocity and thickness and their contribution to the interpretation of the (Young's) modulus in light to the guided wave propagation behavior. Shear wave velocity comparisons highlighted in yellow may have been influenced by nerve thickness and, thus, conclusions about changes in mechanical properties between locations can't be established. Shear wave velocity comparisons highlighted in green indicate that thickness did not influence the shear wave velocity and, consequently, interpretations about spatial variations in mechanical properties can be drawn with confidence.

	Sciatic $_{DISTAL}$	Tibial $_{PROXIMAL}$	Tibial $_{INTERMEDIATE}$	Tibial $_{DISTAL}$
Sciatic $_{PROXIMAL}$	⇧SWV ⇧Thickness ? Modulus	⇧SWV ⇔Thickness ⇧Modulus	⇧SWV ⇩Thickness ⇧Modulus	⇧SWV ⇩Thickness ⇧Modulus
Sciatic $_{DISTAL}$		⇧SWV ⇔Thickness ⇧Modulus	⇔SWV ⇩Thickness ? Modulus	⇧SWV ⇩Thickness ⇧Modulus
Tibial $_{PROXIMAL}$			⇩SWV ⇩Thickness ? Modulus	⇔ SWV ⇩Thickness ? Modulus
Tibial $_{INTERMEDIATE}$				⇧SWV ⇔Thickness ⇧Modulus

SWV: shear wave velocity; Modulus: Young's modulus; ⇧: increase; ⇩: decrease; ⇔: no change; ?: unknown.

adaptations to acute and chronic tensile loads in either healthy (Andrade et al., 2018; Andrade et al., 2020) or impaired (Neto et al., 2020) nerves. These studies have typically examined the shear wave velocity at one single location along the course of sciatic and tibial nerves. This does not account for a potential heterogenous nature of shear waves along the length of lower limb nerves, as shown it has been shown in the upper limbs (Rugel et al., 2020). The present study constitutes the first comprehensive mapping of the human sciatic and tibial nerve shear wave velocity and demonstrates that transducer location should be standardized for accurate comparison between individuals or conditions. The latter is of major clinical importance when assessing impaired peripheral nerves, especially in length dependent neuropathies such as diabetic neuropathy or chemotherapy-induced peripheral neuropathy.

Our observations also showed that hip flexion induced a similar magnitude increase in shear have velocity along the sciatic and tibial nerve. In contrast with our hypothesis, this finding suggests that forces are homogeneously distributed along healthy nerves and well beyond the location where the stress is applied. Future studies are required to determine whether such tensile properties are altered in damaged nerves or in the presence of interfacing injured muscles, as well as their clinical relevance for non-pharmacological rehabilitation strategies (Ellis et al., 2021).

We would like to acknowledge the following methodological considerations. First, the epineurium was excluded from the ROI used to quantify the shear wave velocity. Nevertheless, a recent nerve model suggests a tightly coupled meso-epi-perineurium interacting with a loosely coupled peri-endoneurium (Sung et al., 2019). Therefore, the meso-epineurium connections have the potential to modulate the shear wave velocity of the perineurium, and consequently contribute to the spatial variations observed along the course of the nerve tract. Second, skin marks were used to identify the nerve regions where ultrasound scans were performed. This procedure was performed with the hip in neutral position. However, sciatic and tibial nerve may stretch and slide proximally due to the hip flexion (Boyd et al., 2013; Robinson and Probyn, 2019). It is therefore possible that the scanned nerve locations differed slightly between hip neutral and hip flexion due to nerve sliding. Third, the hip neutral position might not have been sufficient to fully unload the sciatic nerve tract due to the knee (extension) and ankle (neutral) angles. This limitation arises from the methodology adopted in the published randomized controlled study (Andrade et al., 2020), and could explain some of the variability in shear wave velocity observed in hip neutral. In addition, it is possible that the spatial variations could have been influenced by the hip postures adopted in this study. We acknowledge that we have not compared fully unloaded versus loaded nerve configurations. Furthermore, peripheral nerves exhibit longitudinal undulations in both the nerve core and its fascicles that unravel during stretching (Shah, 2017) such as that imposed upon the sciatic nerve tract by the hip flexion. This load-bearing mechanism is likely to modify the overall tissue anisotropy and, thus, to have affected the shear wave velocities. Further studies are required to: 1) compare fully unloaded and loaded sciatic and tibial nerves by manipulating ankle, knee, and hip joints and evaluate their respective usefulness to clinical diagnostic performance; and 2) investigate a larger range of ages.

5. Conclusion

The present study showed spatial-dependent differences in shear wave velocity in the sciatic and tibial nerve. Although shear wave velocity largely increases with the hip flexion along the course of the sciatc and tibial nerve, the spatial variations in nerve shear wave velocity were not altered by nerve tensioning. This further suggest that axial loads are distributed unfirmly along the course of healthy human nerves when subjected to stretching. Overall, our findings contribute to a better understanding of peripheral nerve biomechanics in-vivo. In addition, they demonstrate the importance of considering both transducer location and limb positioning when using ultrasound shear wave elastography for

biomechanical and clinical examinations of the sciatic and tibial nerve.

6. Availability of data and materials

The datasets used are available from the corresponding author on reasonable request.

CRediT authorship contribution statement

Ricardo J. Andrade: Conceptualization, Formal analysis, Investigation, Methodology, Project administration, Visualization, Writing – original draft, Writing – review & editing. **Sandro R. Freitas:** Writing – review & editing, Methodology, Conceptualization. **François Hug:** Conceptualization, Methodology, Writing – review & editing. **Michel W. Coppieters:** Writing – review & editing. **Eva Sierra-Silvestre:** Formal analysis, Writing – review & editing. **Antoine Nordez:** Writing – review & editing, Writing – original draft, Project administration, Methodology, Formal analysis, Conceptualization.

Declaration of Competing Interest

The authors declare that they have no known competing financial interests or personal relationships that could have appeared to influence the work reported in this paper.

Acknowledgements

RJA was supported by a Griffith University Postdoctoral Fellowship Scheme award. This study was financially supported by the Région des Pays de la Loire (QUETE project, no. 2015-09035) and the University of Nantes (Interdisciplinary program). We thank Guillaume Le Sant, Lilian Lacourpaille, Jean-Baptiste Quillard, Sébastien Guillard, Thomas Icre, and Kaoutar Kabbaj for their support in data collection.

References

Andrade, R.J., Freitas, S.R., Hug, F., Le Sant, G., Lacourpaille, L., Gross, R., McNair, P., Nordez, A., 2018. The potential role of sciatic nerve stiffness in the limitation of maximal ankle range of motion. Sci. Rep. 8, 14532.

Andrade, R.J., Freitas, S.R., Hug, F., Le Sant, G., Lacourpaille, L., Gross, R., Quillard, J.-B., McNair, P.J., Nordez, A., 2020. Chronic effects of muscle and nerve-directed stretching on tissue mechanics. J. Appl. Physiol. 129 (5), 1011–1023.

Andrade, R.J., Nordez, A., Hug, F., Ates, F., Coppieters, M.W., Pezarat-Correia, P., Freitas, S.R., 2016. Non-invasive assessment of sciatic nerve stiffness during human ankle motion using ultrasound shear wave elastography. J. Biomech. 49 (3), 326–331.

Bercoff, J., Tanter, M., Fink, M., 2004. Supersonic shear imaging: a new technique for soft tissue elasticity mapping. IEEE Trans. Ultrason. Ferroelectr. Freq. Control 51 (4), 396–409.

Bober, B.G., Shah, S.B., 2015. Paclitaxel alters sensory nerve biomechanical properties. J. Biomech. 48 (13), 3559–3567.

Boyd, B.S., Dilley, A., 2014. Altered tibial nerve biomechanics in patients with diabetes mellitus. Muscle Nerve 50 (2), 216–223.

Boyd, B.S., Topp, K.S., Coppieters, M.W., 2013. Impact of movement sequencing on sciatic and tibial nerve strain and excursion during the straight leg raise test in embalmed cadavers. J. Orthop. Sports Phys. Ther. 43 (6), 398–403.

Bruhn, J., Van Geffen, G.J., Gielen, M.J., Scheffer, G.J., 2008. Visualization of the course of the sciatic nerve in adult volunteers by ultrasonography. Acta Anaesthesiol. Scand. 52, 1298–1302.

Brum, J., Bernal, M., Gennisson, J.L., Tanter, M., 2014. In vivo evaluation of the elastic anisotropy of the human Achilles tendon using shear wave dispersion analysis. Phys. Med. Biol. 59 (3), 505–523.

Çelebi, U.O., Burulday, V., Özveren, M.F., Doğan, A., Akgül, M.H., 2019. Sonoelastographic evaluation of the sciatic nerve in patients with unilateral lumbar disc herniation. Skeletal Radiol. 48 (1), 129–136.

Coppieters, M.W., Alshami, A.M., Babri, A.S., Souvlis, T., Kippers, V., Hodges, P.W., 2006. Strain and excursion of the sciatic, tibial, and plantar nerves during a modified straight leg raising test. J. Orthop. Res. 24 (9), 1883–1889.

Dikici, A.S., Ustabasioglu, F.E., Delil, S., Nalbantoglu, M., Korkmaz, B., Bakan, S., Kula, O., Uzun, N., Mihmanli, I., Kantarci, F., 2016. Evaluation of the Tibial Nerve with Shear-Wave Elastography: A Potential Sonographic Method for the Diagnosis of Diabetic Peripheral Neuropathy. Radiology 282 (2), 494–501.

Ellis, R., Blyth, R., Arnold, N., Miner-Williams, W., 2017. Is there a relationship between impaired median nerve excursion and carpal tunnel syndrome? A systematic review. J. Hand Ther. 30 (1), 3–12.

Ellis, R., Carta, G., Andrade, R.J., Coppieters, M.W., 2021. Neurodynamics: is tension contentious? J Man Manip Ther 30 (1), 3–12.

Gennisson, J.-L., Deffieux, T., Fink, M., Tanter, M., 2013. Ultrasound elastography: principles and techniques. Diagn Interv Imaging 94 (5), 487–495.

Gennisson, J.-L., Deffieux, T., Macé, E., Montaldo, G., Fink, M., Tanter, M., 2010. Viscoelastic and anisotropic mechanical properties of in vivo muscle tissue assessed by supersonic shear imaging. Ultrasound Med. Biol. 36 (5), 789–801.

Greening, J., Dilley, A., 2017. Posture-induced changes in peripheral nerve stiffness measured by ultrasound shear-wave elastography. Muscle Nerve 55 (2), 213–222.

Gustafson, K.J., Grinberg, Y., Joseph, S., Triolo, R.J., 2012. Human distal sciatic nerve fascicular anatomy: implications for ankle control using nerve-cuff electrodes. J. Rehabil. Res. Dev. 49 (2), 309. https://doi.org/10.1682/JRRD.2010.10.0201.

Hadzic, A., 2017. Hadzic's Textbook of Regional Anesthesia and Acute Pain Management. second ed., McGraw-Hill Education.

Hug, F., Tucker, K., Gennisson, J.L., Tanter, M., Nordez, A., 2015. Elastography for Muscle Biomechanics: Toward the Estimation of Individual Muscle Force. Exerc. Sport Sci. Rev. 43, 125–133.

Kantarci, F., Ustabasioglu, F.E., Delil, S., Olgun, D.C., Korkmazer, B., Dikici, A.S., Tutar, O., Nalbantoglu, M., Uzun, N., Mihmanli, I., 2014. Median nerve stiffness measurement by shear wave elastography: a potential sonographic method in the diagnosis of carpal tunnel syndrome. Eur. Radiol. 24 (2), 434–440.

Layton, B.E., Sastry, A.M., Wang, H., Sullivan, K.A., Feldman, E.L., Komorowski, T.E., Philbert, M.A., 2004. Differences between collagen morphologies, properties and distribution in diabetic and normal biobreeding and Sprague-Dawley rat sciatic nerves. J. Biomech. 37 (6), 879–888.

Mahan, M.A., Vaz, K.M., Weingarten, D., Brown, J.M., Shah, S.B., 2015. Altered ulnar nerve kinematic behavior in a cadaver model of entrapment. Neurosurgery 76, 747-755.

Mason, S., Phillips, J.B., 2011. An ultrastructural and biochemical analysis of collagen in rat peripheral nerves: the relationship between fibril diameter and mechanical properties. J. Peripher. Nerv. Syst. 16 (3), 261–269.

Neto, T., Freitas, S.R., Andrade, R.J., Vaz, J.R., Mendes, B., Firmino, T., Bruno, P.M., Nordez, A., Oliveira, R., 2019. Noninvasive Measurement of Sciatic Nerve Stiffness in Patients With Chronic Low Back Related Leg Pain Using Shear Wave Elastography. J. Ultrasound Med. 38 (1), 157–164.

Neto, T., Freitas, S.R., Andrade, R.J., Vaz, J.R., Mendes, B., Firmino, T., Bruno, P.M., Nordez, A., Oliveira, R., 2020. Shear Wave Elastographic Investigation of the Immediate Effects of Slump Neurodynamics in People With Sciatica. J. Ultrasound Med. 39 (4), 675–681.

Paluch, Ł., Noszczyk, B., Nitek, Ż., Walecki, J., Osiak, K., Pietruski, P., 2018. Shear-wave elastography: a new potential method to diagnose ulnar neuropathy at the elbow. Eur. Radiol. 28 (12), 4932–4939.

Phillips, J.B., Smit, X., De Zoysa, N., Afoke, A., Brown, R.A., 2004. Peripheral nerves in the rat exhibit localized heterogeneity of tensile properties during limb movement. J. Physiol. 557, 879–887.

Robinson, L.R., Probyn, L., 2019. How Much Sciatic Nerve Does Hip Flexion Require? Can. J. Neurol. Sci. 46 (2), 248–250.

Rugel, C.L., Franz, C.K., Lee, S.S.M., 2020. Influence of limb position on assessment of nerve mechanical properties by using shear wave ultrasound elastography. Muscle Nerve 61 (5), 616–622.

Schmid, A.B., Coppieters, M.W., Ruitenberg, M.J., McLachlan, E.M., 2013. Local and remote immune-mediated inflammation after mild peripheral nerve compression in rats. J. Neuropathol. Exp. Neurol. 72 (7), 662–680.

Schrier, V.J.M.M., Lin, J., Gregory, A., Thoreson, A.R., Alizad, A., Amadio, P.C., Fatemi, M., 2020. Shear wave elastography of the median nerve: a mechanical study. Muscle Nerve 61 (6), 826–833.

Shah, Sameer, 2017. Tissue Biomechanics: Whales Have Some Nerve. Current Biology 27 (5), 177–179. https://doi.org/10.1016/j.cub.2017.01.054.

Sunderland, S., 1945. The intraneural topography of the radial, median and ulnar nerves. Brain 68 (4), 243–298.

Sunderland, S., 1965. The connective tissues of peripheral nerves. Brain 88 (4), 841–854.

Sunderland, S.S., 1990. The anatomy and physiology of nerve injury. Muscle Nerve 13 (9), 771–784.

Sunderland, S., Ray, L.J., 1948. The intraneural topography of the sciatic nerve and its popliteal divisions in man. Brain 71 (3), 242–273.

Sung, J., Sikora-Klak, J., Adachi, S.Y., Orozco, E., Shah, S.B., 2019. Decoupled epineurial and axonal deformation in mouse median and ulnar nerves. Muscle Nerve 59 (5), 619–628.

Topp, K.S., Boyd, B.S., 2006. Structure and biomechanics of peripheral nerves: nerve responses to physical stresses and implications for physical therapist practice. Phys. Ther. 86, 92–109.

Wang, Q., Zhang, H., Zhang, J., Zhang, H., Zheng, H., 2019. The relationship of the shear wave elastography findings of patients with unilateral lumbar disc herniation and clinical characteristics. BMC Musculoskelet Disord 20, 438.

Watson, J.C., Dyck, P.J.B., 2015. Peripheral Neuropathy: A Practical Approach to Diagnosis and Symptom Management. Mayo Clin. Proc. 90 (7), 940–951.

Wee, T.C., Simon, N.G., 2019. Ultrasound elastography for the evaluation of peripheral nerves: a systematic review. Muscle Nerve.

Zhu, Y., Jin, Z., Luo, Y., Wang, Y., Peng, N., Peng, J., Wang, Y., Yu, B., Lu, C., Zhang, S., 2020. Evaluation of the crushed sciatic nerve and denervated muscle with multimodality ultrasound techniques: an animal study. Ultrasound Med. Biol. 46, 377–392.